Solar Energy Materials & Solar Cells 95 (2011) 1076–1084

Contents lists available at ScienceDirect

Solar Energy Materials & Solar Cells

journal homepage: www.elsevier.com/locate/solmat

The power law *J–V* model of an illuminated solar cell

Shreepad Karmalkar [a,*], H. Saleem [b,1]

[a] Department of Electrical Engineering, Indian Institute of Technology, Madras 600 036, India
[b] Vikram Sarabhai Space Centre, Indian Space Research Organization, Trivandrum 695 022, India

ARTICLE INFO

Article history:
Received 13 July 2010
Received in revised form
30 November 2010
Accepted 3 December 2010
Available online 17 January 2011

Keywords:
Solar cell
J–V model
Peak power point
Closed-form model

ABSTRACT

We have earlier introduced the power law equation, $j=1-(1-\gamma)v-\gamma v^m$, where $j=J/J_{sc}$ and $v=V/V_{\infty}$, to simplify determination of the *J–V* curve, fill-factor and peak power point of an illuminated solar cell from a few measurements as well as physical parameters. However, the validity of the various formulae and parameter extraction procedure was established for a limited class of cells, having moderately convex *J–V* curves with fill-factors of 0.56–0.77 and obeying single exponential theory with bias independent photocurrent. This paper presents a thorough validation of the model proposed earlier. New formulae and parameter extraction procedure are presented to extend the applicability of the power law equation to a much wider variety of cells. The *J–V* curves considered in this paper range from concave (fill-factor <0.25) to highly convex (fill-factor >0.85), and their theoretical expressions contain bias dependent photocurrent and double exponential terms. It is shown that the power law equation also simplifies the calculation of the cell bias point for an arbitrary load.

1. Introduction

In spite of easy availability of computers, device engineers prefer to do preliminary design with simple closed-form formulae which provide physical insight and allow quick back of the paper calculations. Preliminary design of solar cells requires estimates of several quantities from knowledge of either physical parameters (including insolation level and temperature) or measured current density–voltage (*J–V*) data. These quantities are—the bias point (J_L, V_L) for a given load, R_L, the peak power point (J_p, V_p) and the fill-factor (*FF*). Unfortunately, the form of physically based *J–V* models of illuminated solar cells, such as Single Exponential Model (SEM) and Double Exponential Model (DEM), lead to transcendental equations (for these quantities) whose complexity increases for cells having parasitic series and shunt resistances, R_s an R_{sh}, and a bias dependent photocurrent J_{phv} as in polymer [1,2], *a*-Si [3], chalcogenide [4] and some schottky barrier cells [5].

A number of attempts have been made to alleviate the above problem. Refs.[6,7] expressed the SEM in terms of Lambert W function. This expression has the advantages of an explicit form only if the Lambert W function is calculated using an infinite series expansion rather than an iterative algorithm. Moreover, sometimes, either the series does not converge or many terms of the series have to be computed for accuracy. Refs. [8–10] derived explicit models by Taylor's series expansion of an appropriate trial function which has the asymptotic behavior of the SEM under dark conditions for large positive and negative voltages; the process of finding a trial function with correct asymptotic behavior followed by Taylor's series expansion results in a complex explicit form. Also note that all these attempts were restricted to SEM with R_s, and though simplified *J–V* calculations, did not yield closed-form solutions for (J_L, V_L) for a given R_L, (J_p, V_p) and *FF*.

Recently [11], we proposed an explicit Power Law Model (PLM) of a solar cell

$$j=1-(1-\gamma)v-\gamma v^m \text{ where } j=J/J_{sc} \text{ and } v=V/V_{oc}. \quad (1)$$

This equation was shown to allow closed-form estimation of the entire *J–V* curve, (J_p, V_p) and *FF*, both from simple *J–V* measurements and from physical parameters, of a few cells having $0.56\le FF\le 0.77$. The PLM parameters γ and m were expressed in terms of physical parameters assuming a SEM with bias independent J_{ph}.

In this paper, we report new results which expand the scope of the PLM to cover cells having a wide range of material systems and FF <0.25 to >0.85. In Section 2, we provide the analytical motivation behind the form of Eq. (1). Further, we analyze the shapes of the j–v curves generated by Eq. (1) using various combinations of γ and *m*, and show how the PLM realizes a variety of shapes ranging from highly convex curves ($FF>0.85$) of high efficiency cells [12] to concave curves ($FF<0.25$) of recent polymer cells [1,2]. Section 3 presents closed-form formulae in terms of γ and *m* for (J_p, V_p), *FF* and bias point for an arbitrary load. Section 4 derives expressions for γ and *m* in terms of physical parameters of the SEM with bias dependent J_{ph} and the DEM. Section 5 presents extraction of the four PLM parameters from four measured *J–V* bias points. Section 6 discusses the significance of γ and *m* and the prediction of temperature dependence of *FF*. Conclusions appear in Section 7.

* Corresponding author. Tel.: +44 2257 6409; fax: +44 2257 4402.
E-mail addresses: karmal@ee.iitm.ac.in (S. Karmalkar), saleemhaneefa@yahoo.com (H. Saleem).
[1] Tel.: +471 256 5712; fax: +44 241 5236.

0927-0248/$ - see front matter © 2010 Elsevier B.V. All rights reserved.
doi:10.1016/j.solmat.2010.12.005

2. Power law *J–V* equation

The motivation behind the form of the PLM Eq. (1) can be understood by considering its correspondence with the SEM transformed as follows, assuming $J_0 \ll J_{ph}$

$$J \approx \frac{J_{ph}}{1+R_s/R_{sh}} - \frac{V/R_{sh}}{1+R_s/R_{sh}} - \left(\frac{J_0}{1+R_s/R_{sh}}\right)\exp\left(\frac{V+JR_s}{\eta V_t}\right). \quad (2)$$

Here V_t is the thermal voltage, J_0 is the reverse saturation current density, η is the ideality factor, R_s is the parasitic series resistance and R_{sh} is the parasitic shunt resistance. Setting $J=J_{sc}$ for $V=0$ in Eq. (2) and neglecting the term containing J_0/J_{ph}, we get $J_{sc} \approx J_{ph}(1+R_s/R_{sh})$; setting $V=V_{oc}$ for $J=0$, we get $(J_0/J_{ph}) = [1-(V_{oc}/J_{ph}R_{sh})]\exp(-V_{oc}/\eta V_t)$. Dividing Eq. (2) throughout by J_{sc}, substituting the above J_0/J_{ph} expression, and using j and v defined in Eq. (1), we obtain the normalized form of equation

$$j \approx 1-\left(\frac{V_{oc}}{J_{ph}R_{sh}}\right)v-\left(1-\frac{V_{oc}}{J_{ph}R_{sh}}\right)\exp\left[\left(\frac{J_{sc}}{\eta V_t/R_s}\right)j-\left(\frac{V_{oc}}{\eta V_t}\right)(1-v)\right]. \quad (3)$$

This equation has the power law form of Eq. (1) if we take $1-(V_{oc}/J_{ph}R_{sh})=\gamma$ and approximate the exponential term by an explicit power law form as

$$\exp\left[\left(\frac{J_{sc}}{\eta V_t/R_s}\right)j-\left(\frac{V_{oc}}{\eta V_t}\right)(1-v)\right] \approx v^m. \quad (4)$$

Extending this reasoning, we can regard the power law term v^m as an explicit approximation of the sum of two exponentials of the DEM or of more complicated functions, which incorporate bias dependent photocurrent.

Analytical transformation of the left-hand-side of Eq. (4) into the right-hand-side involves a long series of challenging algebraic manipulations. First few steps of this derivation, sufficient to instill confidence in the validity of Eq. (4), are given in Appendix. These steps convert the exponential function into a power law form, with the power m remaining a function of v. Further lengthy algebraic manipulations leading to a power law with constant m independent of v will be dealt with in a separate publication (see Appendix), which will also include bias dependent photocurrent. Moreover, we have found it difficult to algebraically transform the DEM into PLM by a similar approach. Hence, the present paper employs an alternate method to show the ability of the PLM to predict the calculations of all physical models. In this approach, we assume a-priori that the PLM (1) can approximate the results of other physical models because of the shapes of the two model curves are similar, derive γ and m expressions by equating properties such as derivatives of the two models, and establish that simple PLM calculations using the γ, m expressions so derived match the accurate iterative calculations based on SEM with and without bias dependent photocurrent as well as DEM.

The parameters γ and m define the shape of the j-v curve and so, can be called *shape factors*. We can regard γ as the flatness factor, since it is a measure of the flatness of the *J–V* curve near the J_{sc} point, and m as the steepness factor since it is a measure of the steepness of the *J–V* curve near the V_{oc} point. Further discussion of the significance of γ and m appears in the Section 6. Fig. 1(a) and (b) show various shapes of the j–v curve realizable using Eq. (1); the γ and m values leading to these shapes are depicted pictorially in Fig. 1(C) by various regions of the m–γ map. Of the shapes shown, only those for which j is restricted to $0 \le j \le 1$ for $0 \le v \le 1$ are physical. Values of γ and m satisfying this condition are derived in the Appendix as

$$m \ge 0, 0 \le \gamma \le (1-m)^{-1} \text{ for } 0 \le m < 1$$
$$-\infty \le \gamma \le \infty \text{ for } m = 1, -(m-1)^{-1} \le \gamma \le 1 \text{ for } m > 1, \quad (5)$$

and are represented by the hatched region of the m–γ map.

Fig. 1(d) gives the γ and m values obtained by fitting the PLM to measured *J–V* data of as many as 29 cells reported in literature; the wide variety of cells considered can be seen from the range of their V_{oc}, J_{sc}, *FF* and v_p values shown in Fig. 2 and the materials listed in the figure caption. The fit is obtained by minimizing the RMS error $= 100 \times \sqrt{N^{-1}\sum_1^N (\overline{J^i_{PLM}-J^i_{Measured}}/J_{sc})^2}$ between the modelled and measured currents. The magnitude and distribution of the error shown in Fig. 3(a) and the curves (including the one with the worst RMS error) shown in Fig. 3(b) confirm the reasonableness of the fit. The γ and m values of the 29 cells shown in Fig. 1(d) lie in the hatched region of the γ–m map of Fig. 1(c) to the right of the $m=1$ line. Concave curves in Fig. 1(a) and (b) have $\gamma < 0$ and correspond to some polymer cells [30]. We have not come across cells with $m < 1$, i.e. with j–v curves of Fig. 1(b).

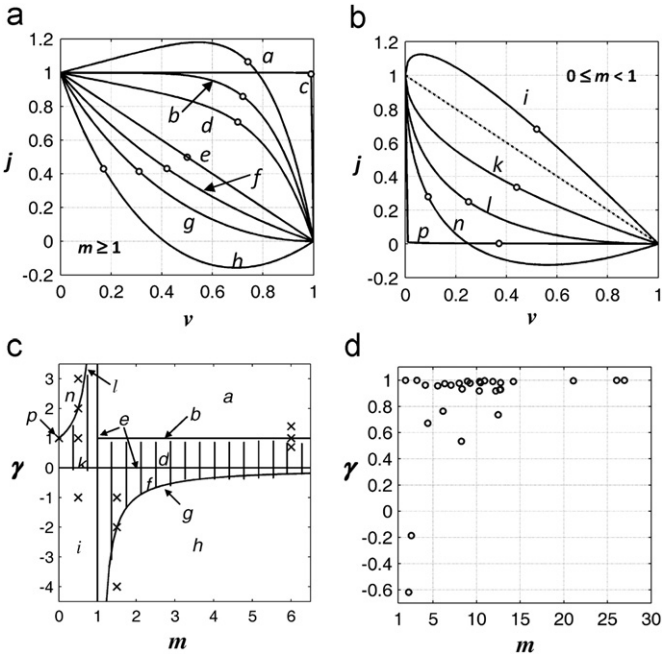

Fig. 1. Shapes of the PLM (1) j–v curves (a) and (b) generated by various regions of the γ–m map (c). For each curve, the values of (γ, m) are indicated on the map by a cross lying in the region having the same label as the curve. The curve '*c*' corresponds to $\gamma=1$ and $m \to \infty$, which lies on the line 'b' of the map far beyond the region shown. Lines '*g*' and '*l*' on the γ–m map represent the two segments of the function $\gamma=(1-m)^{-1}$. (D) γ and m values obtained by fitting the PLM (1) to measured *J–V* data of 29 cells reported in the literature.

3. Bias points and fill-factor in terms of *m* and γ

The normalized peak power voltage, $v_p=V_p/V_{oc}$, is the solution of

$$1-2(1-\gamma)v_p-\gamma(m+1)v_p^m = 0, \quad (6)$$

which is $d(jv)/dv|_{v=vp}=0$, j being given by Eq. (1). Once v_p is obtained, we get the *FF* using $FF=v_pj_p=v_p[1-(1-\gamma)v_p-\gamma v_p^m]$, which increases almost linearly with γ. When the solar cell feeds a load R_L, its bias point (J_L, V_L) is to be solved using $V_L=J_LR_L$ in Eq. (1). The condition $V_L=J_LR_L$ normalizes to $v_L=j_Lr_L$ using $v_L=V_L/V_{oc}$, $j_L=J_L/J_{sc}$, $r_L=R_LJ_{sc}/V_{oc}$, so that v_L is the solution of

$$(1-\gamma+r_L^{-1})v_L+\gamma v_L^m-1 = 0. \quad (7)$$

Thus, the PLM converts implicit equations for v_p and v_L based on SEM or DEM into equations having the following advantage. Although Eqs. (6) and (7) do not have closed-form solutions for general γ, m and r_L, they do have such solutions for specific γ, m and r_L, namely $v_p|_{\gamma=0}=0.5$ and $v_p|_{\gamma=1}=(m+1)^{-1/m}$ in Eq. (6), and $v_L|_{rL\to 0}=r_L$, $v_L|_{rL\to\infty}=1$, $v_L|_{rL=1,m=0}=(1-\gamma)(2-\gamma)^{-1}$, $v_L|_{rL=1,m=1}=0.5$,

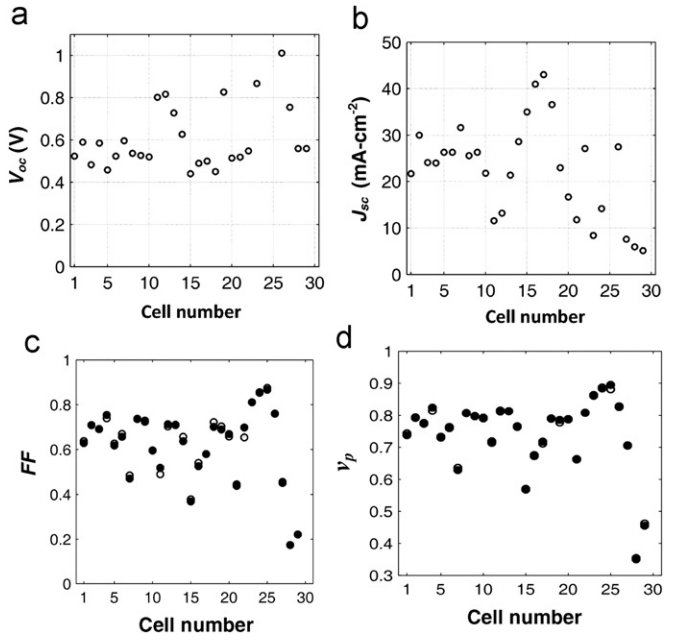

Fig. 2. Open circles show the distributions of the measured parameters of the cells considered in this paper; *Voc*=2.49 V of cell # 24, *Voc*=2.91 of cell # 25 and *Jsc*=3.83 A cm^{-2} for cell # 25 are too high to be shown along with other cells on linear scale. Solid circles show the *FF* and v_p extracted using the analytical four bias points method of presented in Section 5 of this paper, and in most cases, overlap with open circles. The materials of the various cells are as follows: # 1–9: c-Si [13–17], # 10: mc-Si [18], # 11, 12: a-Si [3], # 13: CuInS [19], # 14: CIGS [20], # 15–18: CIS [20,21], # 19: CdTe [22], # 20: Al/SiO2/Si [23], # 21,22: a-SiC:H/c-Si [24, 25], #23: InP [26], #24: GaInP/GaAs (tandem) [27], #25: GaInP/GaInAs/Ge (240x concentrator) [12], #26: GaAs/Ge [28] and #27–29: bulk heterojunction polymer [29,30].

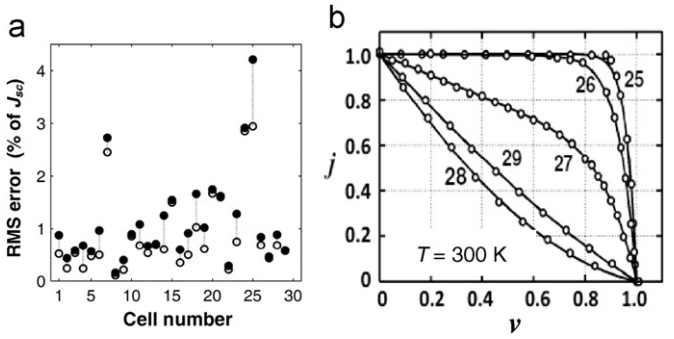

Fig. 3. Illustrating the agreement of the PLM (1) with the measured data. (a) The RMS error between the PLM and measured currents expressed as % of J_{sc}, for the cells of Fig. 2. Open circles correspond to the PLM with minimum RMS error, and solid circles to PLM generated using γ and m extracted by the analytical four bias points method presented in Section 5 of this paper. (b) PLM curves (lines) having minimum RMS error with respect to the measured data (points); the (γ, m, error) values for these curves are: cell # 25 (1.000, 26.0, 2.9%), # 26 (0.990, 14.2, 0.7%), # 27 (0.533, 8.26, 0.4%), # 28 (−0.619, 2.21, 0.7%), # 29 (−0.185, 2.52, 0.6%).

$v_L|_{r_L=1,m=2}=(\sqrt{4+\gamma^2}+\gamma-2)/2\gamma$, $v_L|_{rL=1,m\to\infty}=(2-\gamma)^{-1}$ in Eq. (7). These allow identification of the following simple interpolation formulae $\hat{v_p}$ and $\hat{v_L}$ passing through them (see Appendix for the derivation)

$$\hat{v_p}=(m+1)^{-1/m}-[(m+1)^{-1/m}-0.5](1-\gamma)^{1.58+0.05m}. \quad (8)$$

$$\hat{v_L}=r_L(1+r_L{}^{\alpha})^{-1/\alpha} \quad \alpha=-\log 2/\log v_1 \quad v_1=\frac{1-[\gamma/(1+m^{1.6-0.9\gamma})]}{2-\gamma}. \quad (9)$$

The accuracy of these equations is usually sufficient in practical cases as will be shown shortly. More accurate values, if desired, are obtained using the Newton–Raphson formulae as $v_p=\hat{v_p}-f_p(\hat{v_p})/f'_p(\hat{v_p})$ and $v_L=\hat{v_L}-f_L(\hat{v_L})/f'_L(\hat{v_L})$, where f_p, f_L are the LHS of Eqs. (6) and (7), respectively, and $f'_p f'_L$ are their derivatives with respect to v_p, v_L. The results are

$$v_p=\hat{v_p}-\frac{\gamma(m+1)\hat{v_p}^m+2(1-\gamma)\hat{v_p}-1}{\gamma m(m+1)\hat{v_p}^{m-1}+2(1-\gamma)}, \quad (10)$$

$$v_L=\hat{v_L}-\frac{\gamma\hat{v_L}^m+\hat{v_L}(1-\gamma+r_L{}^{-1})-1}{\gamma m\hat{v_L}^{m-1}+1-\gamma+r_L{}^{-1}}. \quad (11)$$

Ref. [1] gave the solution $v_p\approx(m+1)^{-1/m}-0.05(1-\gamma)$, which becomes grossly inaccurate as γ is lowered from 1, i.e. as the cell quality falls. Fig. 4 compares the results of Eqs. (8) and (10) with numerical calculations using Eq. (6), for $1\le m\le 32$ and physical values of γ (i.e. values satisfying Eq. (5)). The maximum error in Eq. (8) is < 2.5% of V_{oc} for all values of γ considered when $1\le m\le 16$, and < 1% of V_{oc} for $\gamma>0.4$ when $m=32$. The accuracy is much better in practical situations, e.g. see the v_p values of the 29 cells marked in Fig. 4. Use of Eq. (10) reduces the error to < 0.33% of V_{oc} for all values of γ, m. Since the peak of the *jv* versus *v* curves is broad, errors in the *FF* values are significantly smaller than those in v_p.

Fig. 5 compares the results of Eqs. (9) and (11) with numerical calculations for four cells having widely different combinations of γ and m. The proximity of curves *b* and *c* (in Fig. 5) whose m values are close but γ values differ shows the stronger influence of m than γ on v_L–r_L curves. Generally, the cell is biased at the peak power point for maximum insolation and $r_L=v_p/j_p<1$ for this condition; fall in insolation reduces J_{sc} lowering r_L, and so the portion of the v_L–r_L curves for $r_L<1$ is of interest. In this range, the maximum error in Eq. (9) is

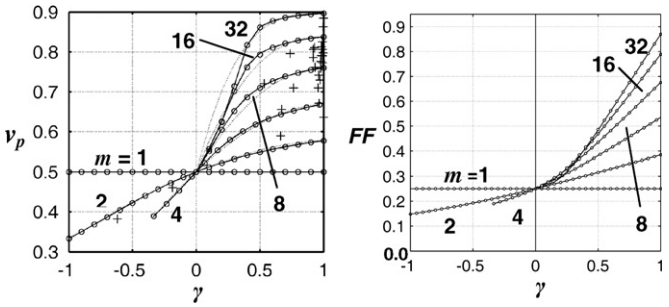

Fig. 4. Results of the v_p and *FF* (lines) compared with numerical calculations (points) based on (1). In the v_p figure, dotted lines are Eq. (8) and solid lines are Eq. (10). The results for the 29 cells are shown using points marked "+"on the v_p graph. The *FF* curves based on Eqs. (8) and (10) overlap.

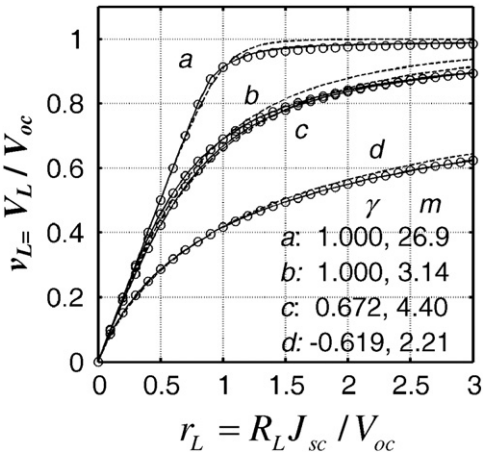

Fig. 5. Bias point for an arbitrary load. Predictions of Eq. (9)—dotted lines, Eq. (11)—solid lines and numerical calculations using Eq. (7)—points are shown. *T*=300 K.

$<2.1\%$ of V_{oc} which is sufficient. Use of Eq. (11) reduces the error to $<1\%$ of V_{oc} for all values of γ and m.

4. Power law model parameters γ, m, J_{sc} and V_{oc} in terms of physical parameters

We derive expressions for γ and m in terms of physical parameters by equating the voltage derivatives of the PLM and the physically based J–V equation at the open-circuit and short-circuit points. This method works for all physically based J–V equations and leads to simple expressions for both γ and m, since all such equations are differentiable, and short-circuit and open-circuit conditions simplify the expression for the derivative. Differentiating the PLM Eq. (1) we get

$$dj/dv|_{v=0} = -(1-\gamma) \text{ leading to } \gamma = 1+dj/dv|_{v=0} \tag{12}$$

and

$$dj/dv|_{v=1} = -(\gamma^{-1}-1+m)\gamma \text{ leading to}$$
$$m = -\gamma^{-1}(dj/dv|_{v=1})+1-\gamma^{-1}. \tag{13}$$

Thus, the derivative at the short-circuit point yields γ and that at the open-circuit point yields m. The expressions for γ and m corresponding to the SEM including bias dependent J_{phv} and DEM are derived below in turn.

4.1. Single exponential model with bias dependent J_{ph}

The J–V expression for this case is

$$J = J_{phv} - J_0[\exp(\overline{V+JR_s}/\eta V_t)-1] - (\overline{V+JR_s}/R_{sh}) \tag{14}$$

where V_t is the thermal voltage, J_0 is the reverse saturation current density and η is the ideality factor. The bias dependence of J_{phv} for various cells are as follows. In a-Si cell [3]

$$J_{phv} = J_{ph\infty}P(1-e^{-1/P}) \text{ where } P = (L_c/D)(1-\overline{V/V_0}), \tag{15}$$

$J_{ph\infty}$ is the maximum photocurrent at far reverse bias, V_0 is the voltage for $J_{ph}=0$, L_c is the collection length and D is absorber layer thickness. In MDMO-PPV:PCBM polymer cell [1]

$$J_{phv} = J_{ph\infty}[\cot h u - u^{-1}] \text{ where } u = (V_0/2V_t)(1-\overline{V/V_0}) \text{ and } J_{ph\infty} = qGL, \tag{16}$$

and in BEH_1BMB_3-PPV:PCBM polymer cell, where J_{phv} is space-charge limited [2]

$$J_{phv} = J_{phsc}\sqrt{1-(V/V_0)} \text{ where } J_{phsc} = qG^{3/4}\sqrt{V_0}(9\varepsilon\mu/8q)^{1/4} \tag{17}$$

G is the generation rate of EHPs, ε is the dielectric constant and μ is the mobility of the slow carrier (usually hole).

Let J_{phoc}, J_{phsc} denote the values of J_{ph} and J'_{phoc}, J'_{phsc} denote the values of $J'_{ph} = dJ_{ph}/dV$ at the open-circuit, short-circuit points, respectively.

In Eq. (14), set $V=0$ and $J=J_{sc}$ to get

$$J_{sc} = \frac{J_{phsc}}{1+R_s/R_{sh}}\left[1-\left(\frac{J_0}{J_{phsc}}\right)\exp\left(\frac{J_{sc}R_s}{\eta V_t}\right)\right] \approx \frac{J_{phsc}}{1+R_s/R_{sh}} \tag{18}$$

Differentiate Eq. (14) with respect to V, set $V=0$ and $J=J_{sc}$, neglect the terms containing the exponentials since $(-V_{oc}+J_{sc}R_s)/\eta V_t$ is a large negative number, and multiply both sides by V_{oc}/J_{sc} and use Eq. (18) to get

$$\left.\frac{dj}{dv}\right|_{v=0} = -\left\{\frac{-(J'_{phsc}V_{oc}/J_{phsc})+(V_{oc}/J_{phsc}R_{sh})+(J_{phoc}/J_{phsc})(1-(V_{oc}/J_{phoc}R_{sh}))(V_{oc}/\eta V_t)e^{((-V_{oc}+J_{sc}R_s)/\eta V_t)}}{1+(J_{phoc}/J_{phsc})(1-(V_{oc}/J_{phoc}R_{sh}))(J_{sc}R_s/\eta V_t)e^{((-V_{oc}+J_{sc}R_s)/\eta V_t)}}\right\} \approx \left(\frac{J'_{phsc}V_{oc}}{J_{phsc}}\right)-\left(\frac{V_{oc}}{J_{phsc}R_{sh}}\right). \tag{19}$$

We substitute Eq. (19) into Eq. (12), and introduce an empirical factor λ to improve accuracy

$$\gamma = 1+\lambda(J'_{phsc}V_{oc}/J_{phsc})-(V_{oc}/\overline{J_{phsc}R_{sh}}). \tag{20}$$

The value of λ depends on the shape of the J_{ph}–V function; sharper the turn in the J_{ph}–V curve, more the difference between J'_{phsc} and the average J'_{ph} in the region near $V=0$, and hence, higher the λ; further explanation of the location and value of λ appears in Appendix. The expressions for various terms (derived from Eqs. (15–17)) are listed in Table 1.

Set $V=V_{oc}$ and $J=0$ in Eq. (14) and assume exponential terms to be $\gg 1$ to obtain the equation for V_{oc}

$$J_0\exp(V_{oc}/\eta V_t)+(V_{oc}/R_{sh})-J_{phoc} \approx 0. \tag{21}$$

Differentiate Eq. (14), set $V=V_{oc}$ and $J=0$, substitute for $J_0\exp(V_{oc}/\eta V_t)$ from Eq. (21), multiply both sides by V_{oc}/J_{sc}, and use Eq. (18)

$$\left.\frac{dj}{dv}\right|_{v=1} = -\left[\frac{-(J'_{phoc}V_{oc}/J_{phsc})+(V_{oc}/J_{phsc}R_{sh})+((J_{phoc}/J_{phsc})-(V_{oc}/J_{phsc}R_{sh}))(V_{oc}/\eta V_t)}{1+((J_{phoc}/J_{phsc})-(V_{oc}/J_{phsc}R_{sh}))(J_{sc}R_s/\eta V_t)}\right]. \tag{22}$$

We substitute Eq. (22) into Eq. (13), simplify the numerator of the resulting expression by expressing $V_{oc}/J_{phsc}R_{sh}$ from Eq. (18),

Table 1
Expressions for the various terms of Eq. (20) for γ and Eq. (23) for m of cells with bias dependent J_{ph} Eqs. (15)–(17). For a-Si cells, $P_{oc} = (L_c/D)(1-\overline{V_{oc}/V_0})$; at $V=0$, $P=L_c/D>1$ and so, we approximate $e^{-D/L_c} \approx 1-(D/L_c)+0.5(D/L_c)^2$. For MDMO-PPV:PCBM polymer cells, $u_{oc} = (V_0/2V_t)(1-\overline{V_{oc}/V_0})$.

Cell	a-Si	MDMO-PPV:PCBM	BEH_1BMB_3-PPV:PCBM
J_{phoc}	$J_{ph\infty}P_{oc}(1-e^{-1/P_{oc}})$	$J_{ph\infty}[\cot h\, u_{oc}-u_{oc}^{-1}]$	$J_{phsc}\sqrt{1-(V_{oc}/V_0)}$
J_{phsc}	$J_{ph\infty}(1-\overline{D/2L_c})$	$J_{ph\infty}(1-\overline{2V_t/V_0})$	$qG^{3/4}\sqrt{V_0}(9\varepsilon\mu/\overline{8q})^{1/4}$
J'_{phoc}	$-\left(\frac{J_{ph\infty}L_c}{V_0D}\right)\left\{1-e^{-1/P_{oc}}\left(\frac{1}{P_{oc}}+1\right)\right\}$	$-(J_{ph\infty}/\overline{2V_t})[\csc h^2 u_{oc}+u_{oc}^{-2}]$	$-(J_{phsc}/\overline{2V_0})[1-(V_{oc}/V_0)]^{-1/2}$
J'_{phsc}	$-J_{ph\infty}D/\overline{2V_0L_c}$	$-2J_{ph\infty}V_t/V_0^2$	$-J_{phsc}/\overline{2V_0}$
λ	1.4+0.09 (L_c/D)	1.4	1.1
δ	1–0.015 (L_c/D)	0	0

assume $(1-\gamma)J_{sc}R_s \ll V_{oc}$ and introduce empirical factors 0.6, δ to improve accuracy

$$m \approx \left(\frac{V_{oc}}{\gamma\eta V_t}\right)\left[\frac{((J_{phoc}/J_{phsc})-(V_{oc}/J_{phsc}R_{sh}))+\delta((\lambda J'_{phsc}-J'_{phoc})/J_{phsc})\eta V_t}{1+0.6((J_{phoc}/J_{phsc})-(V_{oc}/J_{phsc}R_{sh}))(J_{sc}R_s/\eta V_t)}\right]. \quad (23)$$

The factor 0.6 increases m to arrest the underestimation of the current by the PLM at high R_s, and the factor δ reduces m to round-off the corner of the PLM J–V curve for capturing the effect of bias dependent J_{ph}. The locations and values of δ, 0.6 are explained in the Appendix with the help of Fig. 6. The expressions for various terms of Eq. (23) are listed in Table 1. The values of λ, δ given in this table and the value of 0.6 have been verified for a number of cells in the range $0 \le (J_{sc}R_s/\eta V_t) \le 10$, $1 \le \eta \le 3$, $V_0 \le 1$ and $0 \le L_c/D \le 30$ (for a-Si cell).

Fig. 7 shows the good agreement (average RMS error = 0.53%) between the J–V curves of a-Si, MDMO-PPV:PCBM and BEH_1BMB_3-PPV:PCBM cells generated by numerical calculations based on Eqs. (14)–(17) and by the PLM based on Eqs. (1), (18, 20, 21, 23) and expressions of Table 1. The RMS difference between the numerical and PLM calculations of *FF* of the seven cells is 0.005.

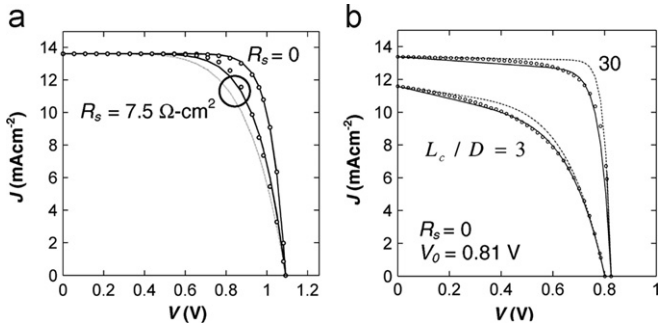

Fig. 6. Illustrating the need for the empirical factors 0.6 (a) and λ, δ (b) in Eqs. (20) and (23) for γ, m of a cell with bias dependent J_{ph}. Solid lines show PLM results with the factors (0.6 in (a) and λ, δ as per Table 1 in (b)), dotted lines show results without the factors, and points show numerical calculations. The calculations are done using $\eta = 2.3$, $R_{sh} = 1\ \text{M}\Omega\ \text{cm}^2$, J_{ph}, $J_{ph\infty} = 13.6\ \text{mA cm}^{-2}$, $J_0 = 2\ \text{nA cm}^{-2}$. The solid and dotted lines overlap for $R_s = 0$ in (a).

4.2. Double exponential model with bias independent J_{ph}

In this case, the J–V model is

$$J = J_{ph} - J_{01}\left[\exp\left(\frac{V+JR_s}{\eta_1 V_t}\right)-1\right] - J_{02}\left[\exp\left(\frac{V+JR_s}{\eta_2 V_t}\right)-1\right] - \frac{V+JR_s}{R_{sh}} \quad (24)$$

Set $V = 0$, $J = J_{sc}$, and neglect the terms containing exponentials compared to $(J_{ph} - J_{sc}R_s/R_{sh})$

$$J_{sc} = J_{ph}(1+R_s/R_{sh})^{-1}. \quad (25)$$

Differentiate Eq. (24) with respect to V, set $V = 0$ and $J = J_{sc}$, neglect the terms containing J_{01} and J_{02}, multiply both sides by V_{oc}/J_{sc}, and use Eq. (25) to get

$$dj/dv|_{v=0} \approx -V_{oc}/\overline{J_{ph}R_{sh}}. \quad (26)$$

Substitute Eq. (26) into Eq.(12) to obtain

$$\gamma = 1 - V_{oc}/\overline{J_{ph}R_{sh}}. \quad (27)$$

Similarly, set $V = V_{oc}$ and $J = 0$ and in Eq. (24), and assume exponential terms to be $\gg 1$, to obtain the equation for V_{oc}

$$J_{01}\exp(V_{oc}/\eta_1 V_t) + J_{02}\exp(V_{oc}/\eta_2 V_t) + \overline{V_{oc}/R_{sh}} - J_{ph} \approx 0. \quad (28)$$

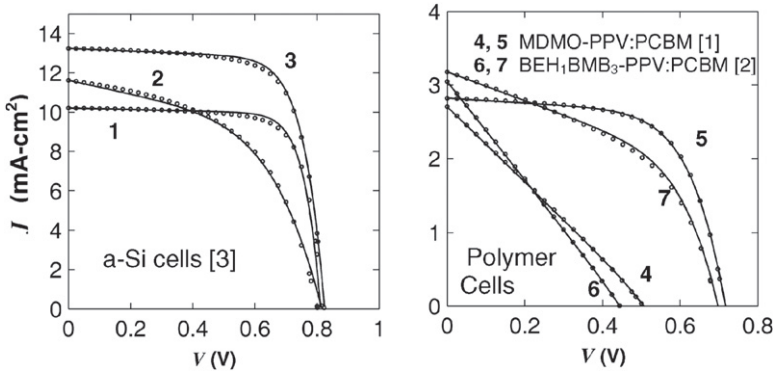

Cell	η	R_s Ω-cm^2	R_{sh} Ω-cm^2	J_0 nA-cm^{-2}	$J_{ph\infty}$ mA-cm^{-2}	V_0 V	L_C/D	FF	γ	m	RMS error %
1	1.54	2.1	1 M	0.007	10.4	0.837	26.8	0.746	0.931	16.3	0.285
2	2.30	2.6	1 M	2	13.6	0.830	3.1	0.518	0.752	6.07	0.394
3	1.54	3.5	1 M	0.007	13.6	0.850	19.0	0.717	0.921	13.7	0.297
4	2.31	8.59	200	13.6	3.0	0.890	---	0.262	0.055	3.57	0.472
5	2.31	8.59	1 M	13.6	3.0	0.890	---	0.645	0.931	8.20	0.712
6	2.31	8.59	200	13.6	--	0.890	--	0.254	0.025	2.21	0.653
7	2.31	8.59	1 M	13.6	--	0.890	--	0.473	0.573	8.48	0.873

Fig. 7. J–V calculations from physical parameters of solar cells with bias dependent photocurrent. Lines show the PLM (1) and points show the numerical calculations. For MDMO-PPV:PCBM cells # 4, 5, $G = 1.56 \times 10^{13}\ \text{cm}^{-3}\ \text{s}^{-1}$, $L = 120$ nm. For BEH_1BMB_3-PPV:PCBM cells # 6, 7, $G = 1.56 \times 10^{21}\ \text{cm}^{-3}\ \text{s}^{-1}$, $\varepsilon = 2.6$, $\mu_h = 3.2 \times 10^{-5}\ \text{cm}^2\ \text{V}^{-1}\ \text{s}^{-1}$. The last column shows RMS error $= 100 \times \sqrt{N^{-1}\sum_1^N \left(\overline{J^i_{PLM} - J^i_{Measured}}/J_{sc}\right)^2}$; $T = 300$ K.

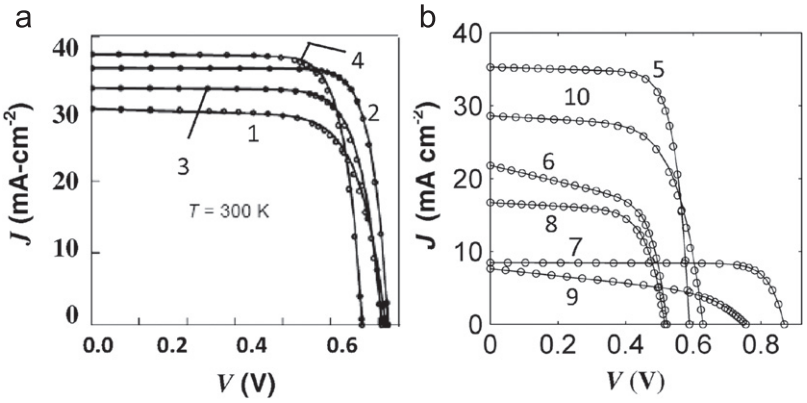

Cell	η_1	J_{01} pA-cm^{-2}	η_2	J_{02} μA-cm^{-2}	R_s Ω-cm^2	R_{sh} kΩ-cm^2	J_{ph} mA-cm^{-2}	*FF*	γ	*m*	RMS error %
1	1.58	8 x10^3	4.00	6.00	0.60	1.10	30.0	0.714	0.962	12.0	1.58
2	1.00	1.33	3.60	0.94	0.34	299	35.6	0.807	0.997	18.7	0.93
3	1.00	1.80	2.00	0.04	0.80	4.50	32.8	0.767	0.992	14.6	2.16
4	1.00	10.0	2.00	0.10	0.40	4.00	37.5	0.773	0.992	16.3	2.09
5	1.34	1.48	--	--	0.19	0.70	35.3	0.760	0.976	15.24	0.73
6	1.27	2.04	--	--	0.63	0.09	22.0	0.597	0.734	13.41	0.70
7	1.44	6x10^{-4}	--	--	0.89	7.91	8.45	0.811	0.987	20.83	0.47
8	1.49	23.9	--	--	1.13	0.39	16.8	0.674	0.921	10.53	1.27
9	2.31	13.6	--	--	8.59	0.20	7.94	0.452	0.506	9.45	1.03
10	2.04	181	--	--	1.16	0.40	28.7	0.658	0.945	8.78	1.65

Fig. 8. *J–V* calculations from physical parameters of DEM (a) and SEM (b); lines show the PLM (1) and points show the numerical calculations. The last column shows RMS error $= 100 \times \sqrt{N^{-1}\sum_1^N \left(j^i_{PLM} - j^i_{Measured}/J_{sc}\right)^2}$ $T=300$ K. Cell materials are # 1–5: c-Si [14,16,31,32], # 6: mc-Si [18], # 7: InP [26], # 8: Al/SiO2/Si [23], # 9: Polymer [29], # 10: CuInGaSe [20]; $T=300$ K.

Differentiate Eq. (24), set $V=V_{oc}$ and $J=0$, substitute for $J_{01}\exp(V_{oc}/\eta_1 V_t)$ from Eq. (28), multiply both sides by V_{oc}/J_{sc}, and use Eq. (25) to get

$$\left.\frac{dj}{dv}\right|_{v=1} = -\left[\frac{(V_{oc}/J_{ph}R_{sh}) + \{1-(V_{oc}/J_{ph}R_{sh}) - (1-(\eta_1/\eta_2))(J_{02}/J_{ph})\exp(V_{oc}/\eta_2 V_t)\}(V_{oc}/\eta_1 V_t)}{1+\{1-(V_{oc}/J_{ph}R_{sh}) - (1-(\eta_1/\eta_2))(J_{02}/J_{ph})\exp(V_{oc}/\eta_2 V_t)\}(R_s J_{sc}/\eta_1 V_t)}\right]. \quad (29)$$

Substitute Eq. (29) into Eq. (13), simplify the numerator of the resulting expression by expressing $V_{oc}/J_{ph}R_{sh}$ in terms of γ from Eq. (27) and assuming $(1-\gamma)J_{sc}R_s \ll V_{oc}$, and multiply the R_s dependent term in the denominator by an empirical factor 0.6 (as in Eq. (23)) to improve the match between PLM and accurate calculations for high values of R_s

$$m \approx \frac{V_{oc}}{\eta_1 V_t}\left[\frac{1-\Delta}{1+0.6\,\gamma(J_{sc}R_s/\eta_1 V_t)(1-\Delta)}\right] \qquad \Delta = \left(1-\frac{\eta_1}{\eta_2}\right)\frac{J_{02}}{\gamma J_{ph}}\exp\left(\frac{V_{oc}}{\eta_2 V_t}\right) \quad (30)$$

Fig. 8(a) shows the good agreement (average RMS error = 1.7%) between the *J–V* curves generated by numerical calculations based on Eq. (24) and by PLM based on Eqs. (1, 25, 27, 30) for four different cells. The need to incorporate the effect of the 2nd exponential term in the model is seen by noting that the RMS errors double if the SEM considering the 1st exponential term alone is used. The RMS difference between the numerical and PLM calculations of the *FF* of the cells is 0.008.

4.3. Single exponential model with bias independent J_{ph}

The expressions for this case were given in [11], and are also obtained as limiting cases of DEM expressions for $J_{02}=0$ or $\eta_1=\eta_2$, i.e. $\Delta=0$, and of SEM expressions with bias dependent J_{phv} for $J_{phoc}=J_{phsc}=J_{ph}$, $J'_{ph}=J'_{phoc}=J'_{phsc}=0$. The expressions for J_{sc} and γ turn out to be same as Eqs. (25) and (27) of the DEM, respectively. The expression for m is repeated here for convenience and highlighting its simplicity

$$m = \frac{V_{oc}/\eta V_t}{1+0.6(\gamma J_{sc}R_s/\eta V_t)} \quad (31)$$

Fig. 8(b) shows the good agreement (average RMS error = 1%) between the *J–V* curves generated by numerical SEM and PLM for six different cells. The RMS difference between the numerical and PLM calculations of the *FF* of the cells is 0.005.

5. Analytical four bias points extraction of power law model parameters γ, m, J_{sc} and V_{oc}

V_{oc} and J_{sc} are measured directly. Two additional measurements are required to estimate γ and m. Values of current and voltage measured at two bias points are substituted in the PLM Eq. (1) to get two equations which are solved simultaneously for γ and m. Suppose we chose the points $v=\alpha$, $j=\alpha$ on the normalized curve, i.e. we measure $J|_{V=\alpha Voc}$, $V|_{J=\alpha Jsc}$ and normalize them with respect to J_{sc}, V_{oc} respectively to obtain $j|_{v=\alpha}$, $v|_{j=\alpha}$ (by way of example, Fig. 9(a) shows these two points for $\alpha=0.6$. Substituting these measured values into Eq. (1), we get the equation

$$j\Big|_{v=\alpha} = 1-(1-\gamma)\alpha-\gamma\alpha^m,\ \ \alpha = 1-(1-\gamma)v|_{j=\alpha}-\gamma(v|_{j=\alpha})^m \tag{32}$$

which lead to

$$\gamma = \frac{j|_{v=\alpha}-1+\alpha}{\alpha-\alpha^m},\ \ m = \frac{\log[(1-\alpha-(1-\gamma)v|_{j=\alpha})/\gamma]}{\log v|_{j=\alpha}}. \tag{33}$$

There are three considerations in the choice of α. First, the $v=\alpha$, $j=\alpha$ points should not be close to either the short-circuit point, where small errors in measured current cause large errors in voltage, or the open-circuit point, where small errors in measured voltage cause large error in current. Second, the four points $v=0$ (short-circuit), $v=\alpha$, $j=\alpha$, and $v=1$ (open-circuit) should be "evenly spaced" to ensure good fit of the PLM to the measured data. This implies that the location of the bias points used to extract γ and m depends on the shape of the j–v curve, i.e. the quality of the cells. Third, it is preferable to chose a value of α for which the α^m term in Eq. (33) can be neglected in comparison to α. This would decouple the extraction of γ from that of m, and avoid an iterative simultaneous solution of these two parameters.

In our earlier work [11], we employed $\alpha=0.6$ (see Fig. 9(a)) and neglected α^m term of the γ expression in Eq. (33), to extract γ and m of good quality cells with $m>10$ and $FF>0.58$. However, the development of cells in a number of material systems reported in literature is at a stage where the cells have much lower values of either m or FF, and at times, the $v=0.6$ and $j=0.6$ are too close to each other. In cells with $m<7.6$, the neglect of the α^m term in the γ expression introduces $>5\%$ error in γ and a corresponding error in m. Moreover, closeness of $v=0.6$ and $j=0.6$ points violates the "even placement" criterion (see Fig. 9(b)) and degrades the fit of the PLM to the measured data. In this paper, we improve the extraction procedure to cover both good as well as poor quality cells. We propose that the points $v=0.6$ and $j=0.6$ be regarded as too close if both $j|_{v=0.6}\le 0.75$ and $v|_{j=0.6}\le 0.75$, and in such a case, $v=0.3$ and $j=0.3$ be used; also, γ and m be should be determined iteratively including the α^m term when $m<7.6$.

The step by step procedure is as follows. We measure bias points $v=0.6$ and $j=0.6$, and extract γ and m using $\alpha=0.6$ and neglecting the α^m term (i.e. assuming $m\to\infty$). The extracted values are appropriate if $m>7.6$ and ($j|_{v=0.6}\ge 0.75$ or $v|_{j=0.6}\ge 0.75$). If $m\le 7.6$ and ($j|_{v=0.6}\ge 0.75$ or $v|_{j=0.6}\ge 0.75$), include the α^m term and determine γ, m iteratively using $\alpha=0.6$. If ($j|_{v=0.6}\le 0.75$ and $v|_{j=0.6}\le 0.75$), measure points $v=0.3$ and $j=0.3$, and calculate γ, m iteratively using $\alpha=0.3$. All iterative calculations begin with an initial guess of $m=\infty$, i.e. neglecting α^m in Eq. (33), and terminate with the calculation of m. The number of iterations = the maximum integer $< 30\alpha^{m-1}$ (a fact arrived at from empirical observations on a large number of cells); for $\alpha=0.6$, the number of iterations is two for $5.5<m\le 6.3$, one for $6.3<m\le 7.6$ and none for $m>7.6$; for $\alpha=0.3$, the number of iterations is two for $2.9<m<3.3$, one for $3.3<m<3.8$ and none for $m>3.8$. In an iteration, if γ exceeds unity which is unphysical, the iterations are terminated, γ is taken to be $=1$ and m is extracted as the value in Eq. (33) for $\gamma=1$. Since the number of iterations is no more than two, the calculations are effectively closed-from.

The efficacy of the above analytical extraction method was confirmed by applying it to the J–V curves reported in the literature for the 29 cells of Fig. 2; bias points with $\alpha=0.3$ were employed for the five cells # 15, 21, 27, 28 and 29 having $FF<0.46$, and $\alpha=0.6$ for the remaining 24 cells; in Fig. 3(b), $\alpha=0.3$ for curves # 27, 28, 29 and $\alpha=0.6$ for curves # 25, 26. For each cell, we compared the analytically extracted values of γ and m with the best fit values shown in Fig. 1(d). The absolute difference between these two values of γ was $<5\%$ for 27 cells and 6, 11% for two cells (# 25,28 of Fig. 3(b)), and values of m was $<5\%$ for 21 cells, 5–10% for 6 cells and 14, 20% for 2 cells # 25, 28 of Fig. 3(b); cell # 25 is highest quality cell ($FF=0.875$) with most convex j–v curve and cell # 28 is the lowest quality cell ($FF=0.171$) with the most concave j–v curve; the RMS difference in γ and m values for the 29 cells was 3% and 6% respectively. It is to be noted that the differences between the RMS error, FF and v_p of analytically extracted and best fit PLM curves, the ultimate quantities of interest, are significantly smaller as shown in Fig. 2(c),(d) and Fig. 3(a). We thus conclude that our extraction method is both effective and efficient: effective because the extracted parameter values are within acceptable error and efficient because method does not require a knowledge of the entire J–V curve but only upto six easily measurable bias points – V_{oc}, J_{sc}, $V|_{J=0.6Jsc}$, $J|_{V=0.6V_{oc}}$, and if latter two are too close, $V|_{J=0.3Jsc}$ and $J|_{V=0.3V_{oc}}$ (essentially, the method generates the entire J–V curve from a knowledge of just four bias points). Extraction of physical parameters – η, J_0, R_s, R_{sh} and J_{ph} – of the SEM from the same four bias points, using PLM, has been discussed elsewhere [33].

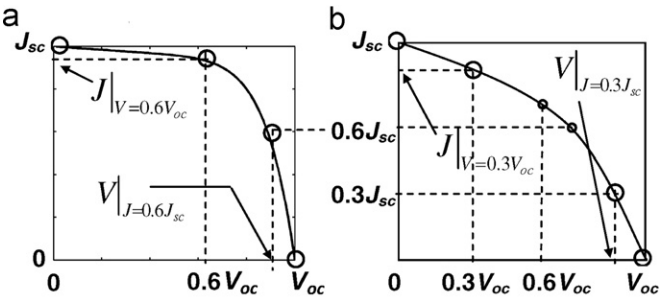

Fig. 9. Four measured points (open circles) on the illuminated J–V curve (line) employed for extracting γ and m of a good quality cell (a) and poor quality cell (b). When $V|_{J=0.6Jsc}$ and $J|_{V=0.6Voc}$ are too close, as may happen in poor quality cells, $V|_{J=0.3Jsc}$ and $J|_{V=0.3Voc}$ are employed.

6. Discussion

Apart from the fact that γ can be regarded as the flatness factor and m as the steepness factor of the j–v curve, these parameters have further significance. The γ–m map of Fig. 1(D) shows that a majority of the cells have γ close to unity, which is a reflection of the fact that R_{sh} is large enough ($\gg V_{oc}/J_{sc}$) in most cells. However, m, which reflects the effect of R_s apart from that of $V_{oc}/\eta V_t$ (e.g. see Eqs. (23) or (30)), is distributed over a wide range of 1–30, showing that, in many cells, R_s is comparable to $\eta V_t/J_{sc}$ and so, more of a problem than R_{sh}. It is further seen from the γ–m map that low $\gamma \Rightarrow$ low m, i.e. a cell with low R_{sh} is likely to have a high R_s as well, and high $m \Rightarrow$ high γ , i.e. a cell with low R_s and η is also likely to have a high R_{sh} (vice-versa are not true). The FF vs γ and FF vs m plots of Fig. 10 show that it is m which correlates to the cell quality. For a cell with $\gamma\to 1$, i.e. R_s alone to be accounted for, Eqs. (1,8,9) simplify to $j=1-v^m$, $v_p=(m+1)^{-1/m}$, $\alpha\approx \ln 2/\ln(1+m^{-0.7})$, respectively, and $FF=m(m+1)^{-1/m-1}$.

In the literature, decrease in cell efficiency and peak power output with temperature have been modeled using a SEM with an ideality factor >1 to account for various current mechanisms; use of SEM is justified as the diffusion current increases more rapidly

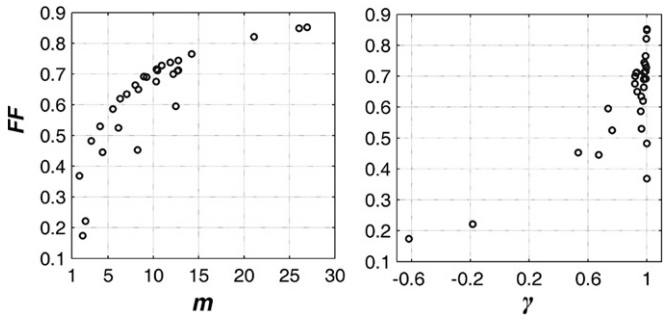

Fig. 10. Correlating the fill-factor to the PLM parameters m and γ.

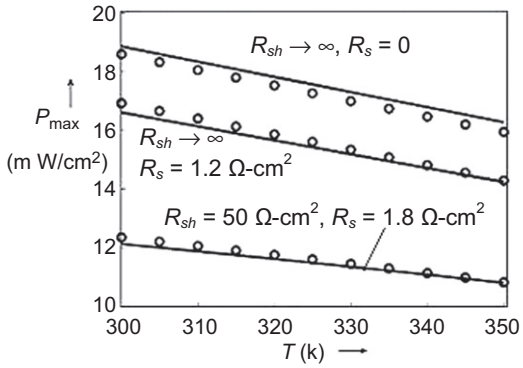

Fig. 11. Temperature dependence of the peak maximum power ($=FF\times V_{oc}I_{sc}$) output of silicon solar cells having $\eta=1.3$, $J_0(300\text{ K})=1\text{ nA cm}^{-2}$, J_{ph} (300 K)=40 mA cm^{-2}, R_s and R_{sh} shown in the figure, $J_{ph}^{-1}(\mathrm{d}j_{ph}/\mathrm{d}T)=0.04\%K^{-1}$ and $J_0(T)=J_0(300\text{K})\exp\left[\frac{E_g}{q\times1.5\times0.025}\left(1-\frac{T}{300}\right)\right]$ or $dV_{oc}/dT\sim-2.4\text{ mV K}^{-1}$. Lines show PLM calculations while points show numerical calculations.

than the current due to other mechanisms and dominates the J–V behavior at higher temperature. Fig. 11 shows the prediction of the temperature dependence of peak power output of silicon cells using the PLM.

7. Conclusion

This paper presents a thorough validation of the power law model of an illuminated solar cell introduced earlier [11]. The model is shown to represent concave to highly convex J–V curves with fill-factors between 0.170 and 0.875 using just four parameters—γ and m, J_{sc} and V_{oc}. Four easily measurable J–V bias points are sufficient to estimate the quantities, namely—peak power point, fill-factor and the entire J–V curve, of a fabricated cell. The power law model simplifies the prediction of these quantities from physical parameters of cells having bias dependent photocurrent and obeying single and double exponential J–V equations. The model also simplifies the calculation of the cell bias point for an arbitrary load, and should be useful for preliminary design.

Appendix

Derivation of Eq. (4): exponential to a power law function transformation

This is based on Ref. [34]. Using α_{sc} and α_{oc} defined below

$$\alpha_{sc}=\frac{J_{sc}}{\eta V_t/R_s},\alpha_{oc}=\frac{V_{oc}}{\eta V_t}, \tag{A1}$$

we can write the left-hand-side exponential term of Eq. (4) as

$$\exp[\alpha_{sc}j-\alpha_{oc}(1-v)]=\exp\{[\alpha_{sc}(j/(1-v))-\alpha_{oc}](1-v)\}. \tag{A2}$$

Since $v<1$, we recognize that

$$\ln v=\ln(1-\overline{1-v})=-(1-v)\delta_v$$
$$\text{where } 1\le\delta_v=1+\frac{(1-v)}{2}+\frac{(1-v)^2}{3}-\cdots\le\infty, \tag{A3}$$

so that

$$1-v=\frac{-\ln v}{\delta_v}. \tag{A4}$$

Substituting (A4) in the RHS of (A2), we can write

$$\exp[\alpha_{sc}j-\alpha_{oc}(1-v)]=\exp\left\{\left[\frac{\alpha_{oc}-\alpha_{sc}(j/\overline{1-v})}{\delta_v}\right]\ln v\right\}=v^m, \tag{A5}$$

where m is the expression multiplying $\ln v$ in (A5), i.e.

$$m=\left(\frac{1}{\delta_v}\right)\left[\alpha_{oc}-\frac{\alpha_{sc}j}{(1-v)}\right] \tag{A6}$$

Further derivation, leading to an effective value of m independent of v that is usable for all v without much loss of accuracy will be given in a separate publication [34], which will also include a bias dependent photocurrent.

Derivation of Eq. (5): conditions on γ and m for physicality of j–v curve

We have $j=1$ at $v=0$, so long as $m\ge0$. To proceed further, we work with the function $dj/dv=\gamma-1-\gamma m v^{m-1}$ which is simpler, and so easier to deal with, rather than Eq. (1). For $0\le v\le1$, the condition $0\le j\le1$ will be satisfied if $\mathrm{d}j/\mathrm{d}v\le0$. Owing to the power law term, $\mathrm{d}j/\mathrm{d}v$ is a monotonically decreasing function for $m>1$, a monotonically increasing function for $m<1$ and a constant$=-1$ for $m=1$. Hence, if $\mathrm{d}j/\mathrm{d}v\le0$ at both the limits $v=0$ and $v=1$, then $\mathrm{d}j/\mathrm{d}v\le0$ over the entire range $0\le v\le1$. Note that $\mathrm{d}j/\mathrm{d}v>0$ at $v=0$ represents a negative R_{sh} in SEM and DEM while $\mathrm{d}j/\mathrm{d}v>0$ at $v=1$ implies that the power law j-v curve has at least one zero in the range $0<v<1$ (see Fig. 1(A) and (B)), both of which are unphysical conditions. For $m>1$, $dj/dv|_{v=0}=\gamma-1\le0$ for $\gamma\le1$ and $dj/dv|_{v=1}=\gamma-1-\gamma m\le0$ for $\gamma\ge-(m-1)^{-1}$ to yield a condition for physicality as $-(m-1)^{-1}\le\gamma\le1$. For $m<1$, $dj/dv|_{v=0}\to-\infty$ for $\gamma>0$, $dj/dv|_{v=0}\to\infty$ for $\gamma<0$ and $dj/dv|_{v=0}=-1$ for $\gamma=0$; in addition, $dj/dv|_{v=1}=\gamma-1-\gamma m\le0$ for $\gamma\le(1-m)^{-1}$ to yield the condition $0\le\gamma\le(1-m)^{-1}$. Finally, for $m=1$, we have $dj/dv|_{v=0}=-1$ independent of the value of γ, so that $-\infty\le\gamma\le\infty$.

Derivation of Eq. (8): peak power point

We can interpolate between the closed-form solutions $v_p|_{\gamma=0}=0.5$ and $v_p|_{\gamma=1}=(m+1)^{-1/m}$ of Eq. (6) as $v_p=(m+1)^{-1/m}-[(m+1)^{-1/m}-0.5]f_\gamma$. Here, the interpolating function $f_\gamma=0,1$ for the limits $\gamma=1,0$ independent of m, and so, is expressed as a power law function of $(1-\gamma)$; the shape of f_γ between the limits, and so, the power, is a weak function of m. Determining the power empirically by fitting to numerical data, we get $f_\gamma=(1-\gamma)^{1.58+0.05\,m}$ leading to Eq. (8).

Derivation of Eq. (9): bias point for an arbitrary load

As per Eq. (7), $v_L\approx r_L$ for small r_L and $v_L\to1$ for $r_L\to\infty$; the sharpness of the transition between these two linear segments is governed by m and γ. A function that fits this behavior and can be used as an initial estimate is given by $\hat{v_L}=r_L(1+r_L{}^{\alpha})^{-1/\alpha}$, where α is a function of m and γ. To derive a simple expression for α, we set $r_L=1$ and equate $\hat{v_L}$ to v_L from Eq. (7) (note that for no other value of r_L can

α be expressed as an explicit function of $\hat{v_L}$). Denoting v_L at $r_L=1$ as v_1, the result is $\alpha=-\log 2/\log v_1$. Solving Eq. (7) for $r_L=1$, we see that v_1 as a function of m increases from $v_1=0.5$ at $m=1$ to $v_1=(2-\gamma)^{-1}$ for $m\to\infty$, and can be interpolated as

$$v_1=(2-\gamma)^{-1}-[(2-\gamma)^{-1}-0.5]f_m=(2-\gamma)^{-1}(1-0.5\gamma f_m). \quad \text{(A7)}$$

Here, the interpolating function $f_m=2$, 1, 0 for $m=0$, 1, ∞, independent of γ (note that Eq. (7) yields $v_1=(1-\gamma)(2-\gamma)^{-1}$ at $m=0$). A function such as $f_m=2(1+m^{\beta})^{-1}$ fits this trend. The shape of f_m between the limits, and so, the power β of m, is a weak function of γ. To determine β, we use the closed-form solution of Eq. (7) at $m=2$ as per which $v_1=(\sqrt{4+\gamma^2}+\gamma-2)/2\gamma$ varies from $(3-\sqrt{5})/2$ at $\gamma=-1$ to $(\sqrt{5}-1)/2$ at $\gamma=1$; consequently, from (A7), $f_m=2(1+2^{\beta})^{-1}$ varies from $7-3\sqrt{5}$to $3-\sqrt{5}$, and so β reduces from 2.55 to 0.69 within the same limits. More detailed calculations reveal this variation of β for $-1\le\gamma\le 1$ to be approximately linear of the form $\beta\approx 1.6$–0.9γ leading to $f_m=2(1+m^{1.6-0.9\gamma})^{-1}$ whose substitution in Eq. (A7) yields the v_1 expression given in Eq. (9).

Derivation of the empirical factors in Eqs. (20) and (23)

The locations and values of the factors λ, δ and 0.6 are derived by comparing the values of γ and m obtained from the formulae (20) and (23) *without these factors* with the best fit values, i.e. values of γ and m which give the best PLM fit to numerical calculations. To simplify matters, this comparison is done using physical parameters which activate a minimum number of terms in Eqs. (20) and (23) apart from the term containing the empirical factor. Consider a cell with $R_{sh}\to\infty$, $J_{phsc}=J_{phoc}=J_{ph}$ and $J'_{phsc}, J'_{phoc}=0$ (see Fig. 6(a)); $\gamma=1$ from Eq. (20) matches with the best fit γ independent of the R_s value; for $R_s=0$, $m=V_{oc}/(\eta V_t)$ from Eq. (23) matches with the best fit m, confirming that neither J_{phoc}/J_{phsc} nor $V_{oc}/(\eta V_t)$ in the numerator of Eq. (23) need empirical correction; for large R_s, $m\approx(V_{oc}/\eta V_t)/[1+(J_{sc}R_s)/(\eta V_t)]$ needs to be raised to match the best fit value and this is achieved by attenuating the R_s dependent term by 0.6. Next, consider an a-Si cell with $J'_{phsc}, J'_{phoc}\neq 0, J_{phsc}\neq J_{phoc}, R_{sh}\to\infty$ and $R_s=0$ (see Fig. 6(b)) for which $\gamma=1+(J'_{phsc}V_{oc}/J_{phsc})$ needs to be corrected for both low and high L_c/D values, and this is achieved by multiplying the J'_{phsc} dependent term by λ; including this factor in the m formula as well, we get $m\approx(V_{oc}/\eta V_t)[(J_{phoc}/J_{phsc})+(\lambda J'_{phsc}-J'_{phoc})(\eta V_t/J_{phsc})]$ which matches with the best fit value for low L_c/D but needs correction for high L_c/D, and this is achieved by multiplying the $(\lambda J'_{phsc}-J'_{phoc})$ term by δ (neither J_{phoc}/J_{phsc} nor $V_{oc}/(\eta V_t)$ can be corrected for reasons given above). In polymer cells where there is no L_c/D term, the values of λ and δ are constant.

References

[1] V.D. Mihailetchi, L.J.A. Koster, J.C. Hummelen, P.W.M. Blom, Photocurrent generation in polymer-fullerene bulk heterojunctions, Phys. Rev. Lett. 93 (2004) 216601.1–216601.4.

[2] V.D. Mihailetchi, J. Wildeman, P.W.M. Blom, Space-Charge Limited Photocurrent, Phys. Rev. Lett. 94 (2005) 126602.1–126602.4.

[3] S. Hegedus, J.E. Philips, Parametric analysis of a-si solar cells from current voltage measurements, in: Proceedings of the Conference Record First WCPEC, Hawaii, 1994 pp. 664–667.

[4] M. Gloeckler, C.R. Jenkins, J.R. Sites, Explanation of light/dark superposition failure in CIGS solar cells, Proc. Mat. Res. Soc 763 (2003) 231–236.

[5] S. Niemcharaoen, K. Kobayashi, M. Kimura, K. Sato, Voltage dependence of photocurrent in metal-semiconductor-metal structures under front-illuminated conditions, Solid-State Electron 45 (2001) 1815–1819.

[6] A. Jain, A. Kapoor, Exact analytical solutions of the parameters of real solar cells using Lambert *W*—function, Sol. Energy Mater. Sol. Cells 81 (2004) 269–277.

[7] T.C. Banwell, A. Jayakumar, Exact analytical solution for the current flow through diode with series resistance, Electron. Lett. 36 (2000) 291–292.

[8] A. Ortiz-Conde, F.J. Garcia Sanchez, Approximate analytical expression for equation of ideal diode with series and shunt resistances, Electron. Lett. 28 (1992) 1964–1965.

[9] M.T. Abuelma'atti, Improved approximate analytical solution for generalized diode equation, Electron. Lett. 28 (1992) 594–595.

[10] T.A. Fjeldly, B.J. Moon, M.S. Shur, Approximate analytical solution of generalized diode equation, IEEE Trans. Electron Devices 38 (1991) 1976–1977.

[11] S. Karmalkar, S. Haneefa, A physically based explicit *J–V* model of a solar cell for simple design calculations, IEEE Electron Device Lett. 29 (2008) 449–451.

[12] R.R. King, D.C. Law, K.M. Edmondson, C.M. Fetzer, G.S. Kinsey, H. Yoon, R.A. Sherif, N.H. Karam, 40% eficient metamorphic GaInP/GaInAs/Ge multijunction solar cells, Appl. Phys. Lett. 90 (2007) 183516.1–183516.5.

[13] J.P. Charles, M. Abdelkrim, Y.H. Muoy, P. Mialhe, A practical method of analysis of the current–voltage characteristics of solar cells, Sol. Cells 4 (1981) 169–178.

[14] M. Lipinski, P. Panek, R. Ciach, J. Optoelectron, The industrial technology of crystalline silicon solar cells, J. Optoelectron Adv. Mater. 5 (2003) 1365–1371.

[15] E. Radziemska, Thermal performance of Si and GaAs based solar cells and modules: a review, Prog. Energy Combust. Sci. 29 (2003) 407–424.

[16] D.S. Chan, J.R. Phillips, C.H. Phang, A comparative study of extraction methods for solar cell model parameters, Solid State Electron. 29 (1986) 329–337.

[17] K. Bouzidi, M. Chegaar, A. Bouhemadou, Solar cells parameters evaluation considering the series and shunt resistance, Sol Energy Mater. Sol. Cells 91 (2007) 1647–1651.

[18] S. Ray, Thin Film Solar Cells with microcrystalline silicon as absorber layer, in: Proceedings of the International Workshop on Physics Semiconductor Devices, 2003, pp. 887–891.

[19] J. Klaery, J. Bruns, R. Henninger, K. Siemer, R. Klenk, K. Ellmer, D. Braunig, Efficient $CuInS_2$ thin-film solar cells prepared by a sequential proces, Semicond. Sci. Technol. 13 (1998) 1456–1458.

[20] J.R. Tuttle, M. Contreras, A. Tennant, D. Albin, R. Noufi, High efficiency thin-film Cu(In,Ga)Se_2—based photovoltaic devices: progress towards a universal approach to absorber fabrication, in: Proceedings of the 23rd IEEE Photovoltaic Specialists Conference, 1993, pp. 415–421.

[21] H. Du, C.H. Champness, I. Shih, Results on monocrystalline $CuInSe_2$ solar cells, Thin Solid Films 480 (2005) 37–41.

[22] L. Feng, J. Zhang, B. Li, W. Cai, Y. Cai, L. Wu, W. Li, J. Zheng, Q. Yan, G. Xia, D. Cai, The electrical, optical properties of cdTe polycrystalline thin tilms deposited under Ar–O_2 mixture atmosphere by close-spaced sublimation, Thin Solid Films 491 (2005) 104–109.

[23] S. Altındal, A. Tataroglu, I. Dokme, Density of interface states, excess capacitance and series resistance in the metal–insulator–semiconductor (MIS) solar cells, Sol. Energy Mater. Sol. Cells 85 (2005) 345–358.

[24] J. Pallares, R. Cabre, L.F. Marsal, R.E.I. Schropp, A compact equivalent circuit for the dark current–voltage characteristics of nonideal solar cell, J. Appl. Phys. 100 (2006) 084513.1–084513.5.

[25] M.M. Rahman, S. Furukawa, Amorphous/crystalline heterostructure as a novel approach to fabrication of a solar cell, Electron. Lett. 20 (1984) 57–58.

[26] C. Goradia, W. Thesling, Key factors limiting the open circuit voltage of n^+pp^+ indium phosphide solar cells, in: Proceedings of the 21st IEEE Photovoltaic Specialists Conference, 1, 1990, pp. 386–393.

[27] T. Takamoto, E. Ikeda, H. Kurita, Over 30% efficient InGaP/GaAs tandem solar cells, Appl. Phys. Lett. 70 (1997) 381–383.

[28] S. Shah, S. Tripathy, M. Thirumavalavan, A.T. Kalghatgi, S.B. Krupanidhi, Device processing and *I–V* parameter extraction of MOCVD grown GaAs/Ge heterostructure solar cells, in Proceedings of the 13th International Workshop on Physics Semiconductor Devices, Chennai, 2003.

[29] T. Jeranko, H. Tributsch, N.S. Sariciftci, J.C. Hummelen, Patterns of efficiency and degradation of composite polymer solar cells, Sol. Energy Mater. Sol. Cells 83 (2004) 247–262.

[30] A.T. Mallajosyula, S.S.K. Iyer, B. Mazhari, Fill factor and short circuit current improvement in P3HT:PCBM solar cells incorporating single walled carbon nanotubes, in: Proceedings of the 15th International Workshop on Physics Semiconductor Devices, New Delhi, 2009, pp. 1200–1203.

[31] N. Veissid, D. Bonnet, H. Richter, Experimental investigation of the double exponential model of a solar cell under illuminated conditions: considering the instrumental uncertainties in the current, voltage and temperature values, Solid State Electron. 38 (1995) 1937–1943.

[32] A. Kaminski, J.J. Marchand, A. Laugier, ideal dark I-V curves behavior of silicon solar cells, Sol. Energy Mater. Sol. Cells 51 (1998) 221–231.

[33] H. Saleem, S. Karmalkar, An analytical method to extract the physical parameters of a solar cell from four points on the illuminated *J–V* curve, IEEE Electron. Device Lett. 30 (2009) 349–352.

[34] A. K. Das, S. Karmalkar, Analytical derivation of the closed- form power law J-V model of an illuminated solar cell from the physics based implicit model, accepted for publication in IEEE Trans. Electron Devices.